Heliyon 7 (2021) e07113

Contents lists available at ScienceDirect

Heliyon

journal homepage: www.cell.com/heliyon

Research article

Effect of the Na_2O–Nb_2O_5–P_2O_5 glass additive on the structure, dielectric and energy storage performances of sodium niobate ceramics

S. Benyounoussy [a,*], L. Bih [b,c], F. Muñoz [d], F. Rubio-Marcos [e,f], A. EL Bouari [a]

[a] Laboratory of Physico-chemical of Applied Materials, Faculty of Sciences Ben M'Sik, Hassan II University, Casablanca, Morocco
[b] Materials and Processes Department, ENSAM Meknes, Moulay Ismail University, Meknes, Morocco
[c] Physico-Chemistry Condensed Matter (UPMC) Team, Faculty of Sciences of Meknes, University Moulay, Ismail, Morocco
[d] Institute of Ceramics and Glass (CSIC), Kelsen 5, 28049 Madrid, Spain
[e] Electroceramic Department, Instituto de Cerámica y Vidrio, CSIC, Madrid 28049, Spain
[f] Escuela Politécnica Superior, Universidad Antonio de Nebrija, C/Pirineos, 55, 28040, Madrid, Spain

ARTICLE INFO

Keywords:
Phosphate glasses
Sodium niobate
Composite
Dielectric features
Energy storage performance

ABSTRACT

A phosphate glass Na_2O–Nb_2O_5–P_2O_5 (NPP) is incorporated into $NaNbO_3$ (NN) ceramics to examine its impact on the density, rearrangement of structural units, dielectric and energy storage features of the elaborated composites. The sodium niobate ceramic (NN) is prepared using the solid state process, whereas, the Na_2O–Nb_2O_5–P_2O_5 (NPP) glasses are produced using the method of conventional melt quenching. The glass (NPP) is added to the ceramic (NN) according to the composition (100-x) NN-xNNP; (x = 0, 2.5, 5, and 7.5 %wt). The developed composites are denoted as NN-Gx where x represents the content of glass in %wt. The appropriate sintering temperature for the glass-ceramic composites was measured based on the density measurements. It was found that with the addition of glass, their density was decreased and their fritting at lower temperatures was enhanced. The obtained SST for all composites is about 900 °C. After the densification stage, Raman spectroscopy, X-ray Diffraction, Granulo-laser analysis, and scanning electron microscopy are examined to study the structural approach and the morphology of sintered NN-Gx composites. The NN-G5 composite was found to have a fine grain microstructure that was uniform. The dielectric features of the composite revealed that at ambient temperature the NN-G5 had the greatest dielectric constant. The energy storage performance of the composite was investigated from the P-E plots and the parameters of energy storage. Based on the obtained results, it was concluded that incorporating up to 5% wt. of NNP glass in sodium niobate ceramics positively affects their dielectric and energy storage performances.

1. Introduction

Many perovskite structure materials have been used as dielectrical devices to store energy for high-density capacitors. Sodium niobate ceramic $NaNbO_3$ (NN) is considered one of them owing to their exceptionally large permittivity and their weak dielectric loss [1]. The pure $NaNbO_3$ ceramics produced using the conventional solid-state method exhibit the presence of pores between the grains, as NN grain boundaries generally migrate resulting in the growth of grains. The maximum polarization of these ceramics was very high, and the remnant polarization was quite low. Unfortunately, the existence of the defect as pores and grain boundaries in those materials makes their dielectric breakdown strength very limited at about (100 kV/cm) [2].

To reduce the pores and improve the NN ceramics total energy storage, it is necessary that these materials' dielectric permittivity must be increased while defects must be minimized. Several researchers have thought of improving these properties by adding oxides or glasses to the NN ceramic in order to produce a composite having a high dielectric constant with low dielectric losses and high energy storage density. For instance, the improvement of the energy storage performance of lead-free $NaNbO_3$-based ceramics by adding Bi_2O_3 is reported [3]. The authors were introduced the Bi_2O_3 into $NaNbO_3$ in order to increase the energy storage density of the ceramic. It was found about 4.03 $J.cm^{-3}$ with energy efficiency (η) of 85.4% at 250 kV cm^{-1}. It is worth noticing that, the frequency, temperature stability, and fatigue endurance were found excellent also. Similar work on the introduction of Bi^{3+} at A-site and Mg^{2+} at B-site of the ceramic $NaNbO_3$ (BMN) was reported. It was found that the composition of 0.85NN-0.15BMN had an energy storage density of 2.7 $J.cm^{-3}$ with a yield of 90% [4]. In order to develop a composite having an excellent dielectric constant and a high dielectric strength,

* Corresponding author.
E-mail address: sanaa.benyounoussy@gmail.com (S. Benyounoussy).

https://doi.org/10.1016/j.heliyon.2021.e07113
Received 17 December 2020; Received in revised form 17 February 2021; Accepted 17 May 2021

barium titanate ceramic ($BaTiO_3$) was added to $NaNbO_3$ ceramic [5]. The results indicated that the microstructure of the sample changed, while the density and the dielectric constant increased. Research on energy storage improvement for NN ceramic by adding glass is still very limited in contrast to the $LiNbO_3$ [6], $BaTiO_3$ [7], $Ba_xSr_{1-x}TiO_3$ [8], and other dielectric materials. The common result of all these works indicates that incorporating glass to specific dielectric ceramics may considerably influence fritting temperature, as well as the microstructure, the dielectric and energy storage characteristics. So, one can note that the nature of the glass and its electrical character have a major impact on these properties. For this reason, it is necessary to choose carefully the composition of the glass to be added. There have been a few research studies on NN phosphate composites that we are aware of. As a result, this research work is centered on developing new composites based on NN phosphate.

The nature of the glass and its electrical activity have a significant impact on the dielectric properties of NN composites. To develop phosphate glasses that should keep the strongest possible permittivity of the phosphate-NN composites, a selection strategy is carried out. To reach this objective, we have examined glasses in the ternary system Na_2O–Nb_2O_5–P_2O_5 that contain the identical chemical components as NN. After that, we have investigated their crystallization in the context of heating treatments. Then, using the XRD technique, we focused on identifying chemical compositions that enable the formation of the $NaNbO_3$ phase in glass-ceramics. We have detected that $25Na_2O$–$25Nb_2O_5$–$50P_2O_5$ glass reveal the formation of NN embedded in the glass matrix. The effect of this NNP glass on the structural, the dielectric and the energy storage features of NN composites have been the subject of our research.

2. Experimental procedure

$NaNbO_3$ (NN) (Na: Nb = 50: 50) was made using solid-state reaction process using high purity Na_2CO_3 (Fisher Scientific; >99%) and Nb_2O_5 (Fisher Scientific; ≥99.5%). Both raw materials raw materials balanced in suitable proportions, were completely mixed and calcined at different temperatures. The mixtures were then treated for 2 h at 1200 °C.

Phosphate glass of composition $50Na_2O$–$25Nb_2O_5$–$25P_2O_5$ was prepared using the melt-quench technique. It was elaborated from high purity powders of $NH_4H_2PO_4$, Nb_2O_5, and Na_2CO_3 purchased from Fisher Scientific. The mixture was melted at 1100 °C and then quenched in the air to get the glass. The obtained glass was heated at 300 °C for 2 h to eliminate residual stresses, then crushed to a fine powder in a mortar. In this work, the glass composition with high niobium content (y = 25 mol %) (NNP) was considered according to its dielectric characteristics.

In order to obtain the composites, the NNP glass was added to the NN ceramic according to the chemical compositions (100-x) NN-xNNP (x = 0, 2.5, 5, 7.5 mol %) followed by thorough mixing. The (100-x) NN-xNNP mixed powder was calcined at 500 °C for 4h and sintered in an electric furnace at different temperatures for 2 h. The elaborated ceramics were labeled as NN-Gx, where x represents the batched glass concentration (NN-G0, NN-G2.5, NN-G5, and NN-G7.5).

The density of the samples (ρ) was measured by the standard Archimedes method using water as the immersion liquid. The accuracy of the measurement was 0.02 $g.cm^{-3}$. Raman spectra of the ceramic composites were recorded using DXR2 Raman spectrometer with 633 nm laser excitation. The spectra were acquired in a backscattering geometry in the range of wavelengths 200-1400 cm^{-1}. The ceramics XRD patterns were registered with a Bruker D8 discover employing a Kα (Cu) radiation with a step size of 0.01°. Mastersizer 2000, Hydro 2000G (A) accessory (Malvern instruments) granule-laser was used to measure powder particle size distribution of synthesized composite. Microstructural observations were performed on unpolished samples using a field emission scanning electron microscopy Minisem Hirox SH-4000M Detector Model SED being operated in secondary electron imaging mode. The dielectric measurements for ceramic composites were studied by using Solartron Analytical ModuLab XM MTS in the temperature range of 27–300 °C and working in the frequency range 1Hz to 1MHz. The (P–E) hysteresis loops were measured at room temperature using a ferroelectric tester (RT6000HVA, Radiant Technology, Histersimetro). All the ceramic composites samples were immersed in silicon oil to prevent flashover.https://www.cnrtl.fr/definition/aigu%C3%AB.

3. Results and discussion

3.1. Density measurements

The variation of apparent density with sintering temperature was calculated to determine the appropriate sintering temperature (SST) of the new NN-Gx composites (x = 0, 2.5, 5, 7.5 wt %), which ranged from 800 to 1000 °C as is shown in Figure 1. It may be noted that the values of the density depend on the glass content in the NN ceramic as well as the fritting temperatures. For example at a fixed sintering temperature, it is observed that as the glass ratio in composites is increased, the density values decrease. This may be due to the replacement of a denser $NaNbO_3$ ($\rho = 4.45$ g/cm^3) by the glass phase that has a weaker density ($\rho = 2.72$ g/cm^3) compared to the $NaNbO_3$ phase. This decrease can also be related to the incorporation of a lighter component NNP glass (132.93 g/mol) in the structure instead of the heavier $NaNbO_3$ (163.96 g/mol). Figure 1 showed the effect of the sintering temperature on the density. It reveals that the density is also temperature-dependent and exhibits a maximum at 900 °C. The density of the samples sintered at 900 °C is higher than those sintered at 800 °C and 1000 °C. Similar results were reported in borate and silicate-based ceramic composites [8]. This can be demonstrated by the molten state of the added glass that penetrates the pores between the NN grains [9]. In the present work, the suitable sintering temperature (SST) to have a less porous composite with a high density was found to be 900 °C. This result will be confirmed by the SEM micrographs in Figure 4.

3.2. Raman spectroscopy

In order to shed more light on the structural changes in the (1-x) NN-xNNP composites, their Raman spectra have been carried out in the range of wave numbers from 100 to 1400 cm^1 as indicated in Figure 2.

Firstly, the NNP glass Raman spectra shows several bands situated in the frequencies of 215–550 cm^{-1}, 635 cm^{-1},815 cm^{-1}, 895 cm^{-1}, and 1040 cm^{-1}. The bands in the frequency range of 215–550 cm^{-1} are associated with the bending vibrations of the phosphate and niobium polyhedrons [10]. The others that appeared at 635 and 815 cm^{-1} can be attributed to Nb–O vibrational modes in the NbO_6 octahedra. As a matter

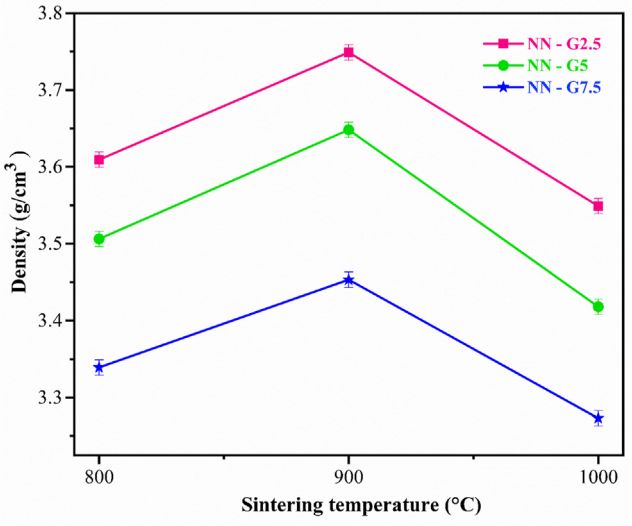

Figure 1. Bulk density of the (100-x)NN-xNNP ceramics as function of the sintering temperature.

of fact, the band at 635 cm^{-1} is relative to the Nb–O stretching mode of corner shared octahedral while the one at 815 cm^{-1} corresponds to Nb–O vibrations in chains like NbO_6 octahedra. The peak positions at 1160 cm^{-1} and 1040 cm^{-1} correspond to the symmetric stretching vibration of $(PO_2)^-$ in metaphosphate and $(PO_3)^{2-}$ in pyrophosphate entities, respectively. Thus, the structure of the glass NNP contains niobium in octahedral sites within the phosphate glassy network composed by metaphosphate and pyrophosphate structural units. The niobium ion was shown to adopt an octahedral geometry with oxygen and forms either Nb–O–P and/or Nb–O–Nb linkages.

Secondly, the NN ceramic Raman spectrum displays very similar vibrational modes to those of the previously reported Raman studies on $NaNbO_3$ ceramics [11]. The bands at 183 cm^{-1}, 1246153 cm^{-1} and 76 cm^{-1} are attributed to the Na^+ translational modes [12]. As seen in Figure 2, the main signals of NN ceramic are around 874 cm^{-1}, 609 cm^{-1}, 576 cm^{-1},434 cm^{-1}, 225-280 cm^{-1} and 204 cm^{-1}. The bands below 350 cm^{-1} are attributed to the $\nu 5$, $\nu 6$ vibrations, and the ions NbO_6 liberation mode. While the other ones above 350 cm^{-1} are associated with the $\nu 4$, $\nu 2$, $\nu 1$, and to the combination $\nu 5 + \nu 1$ vibrations of the NbO_6 group. All the cited vibration modes of NbO_6 octahedron indicate that the perovskite phase $NaNbO_3$ has been formed [13, 14].

Thirdly, the analysis of the Raman spectra of the composites is made regarding the NNP glass and NN ceramic data. It can be inferred that the orthorhombic structure of the NN phase was well preserved in the composites samples. The addition of NNP glass to NN ceramic with 2.5, 5, and 7.5 wt % did not influence the peak position of the $NaNbO_3$ phase but it decreases the band's intensity. It is noticed that the bending mode of the phosphate (PO_4) tetrahedron appears in the range 344–490 cm^{-1}. It seems that the decrease in the Raman band's intensity is due to the substitution of the crystalline NN by the amorphous phase [15].

3.3. XRD analysis

The x-ray diffraction patterns of the composites are carried out in order to seek more structural information about them. Figure 3 represents the x-ray diffraction patterns of NN-Gx composites with different amounts of glass sintered at 900 °C. The XRD patterns of the NN ceramic are associated with a pure $NaNbO_3$ perovskite phase (PDF # 01-073-0803). It is shown that the NN phase is dominating in all composites NN-Gx due to a small content of NNP glass existed in the ceramics. With the addition of glass from 2.5 to 7.5 wt %, a new crystalline phase of $NaPO_3$ with (PDF # 00-011-065) appeared. As compared to $NaNbO_3$, the peaks of the $NaPO_3$ peak are very small. The formation of this phase is due to structural rearrangements within the NNP glass and its crystallization during the sintering of NN-Gx ceramics. It is seen that the peak intensity of the NN phase increased in all ceramic composites, which can be explained by the crystallization of the $NaNbO_3$ phases.

Furthermore, based on the diffraction peak broadening, and using the Scherrer formula, the NN phase crystallite size may be determined as indicated in Eq. (1) [16]:

$$Dp = \frac{k.\lambda}{B.\cos\theta} \quad (1)$$

Where Dp is the average crystallite size, K is the Scherrer constant, λ is the X-ray wavelength (0.15406 nm) and B is the Full Width at Half Maximum of XRD peak.

The crystallite size of the pure NN sample was estimated to be 30.37 nm, and it gradually reduced when NNP glass was added, reaching 29.02 nm in NN-G2.5, 27.51 nm in NN-G5, and 28.77 nm in NN-G7.5. The average crystallite size estimates are consistent with the literature [17, 18]. Based on this result, it can be concluded that the median crystallite size of the NN phase decreased with the addition of NNP glass until 5 mol %.

3.4. Microstructure analysis

It is well known that the microstructural features play an important role in the functional characteristics of the Ferro-ceramics and, therefore, their morphology and distribution can be used to plan new strategies in designing new composite materials with improved functional properties. From this perspective, the relationships between microstructure are studied here using the SEM micrograph, as shown in Figure 4. Figure 4 (a) relative to the pure NN phase showed a dense and intergranular porous microstructure with a large grain size. Most of the grains have an angular appearance with plane interfaces. Smaller grains were also observed in NN ceramic. The addition of NNP glass to the NN ceramic affects its microstructure as shown in Figure 4 (b-d). With the increase in the glass content, it is observed that grain size and pore size decreased from the NN-G2.5 to NN-G5. The incorporation of 2.5 wt % of NNP glass

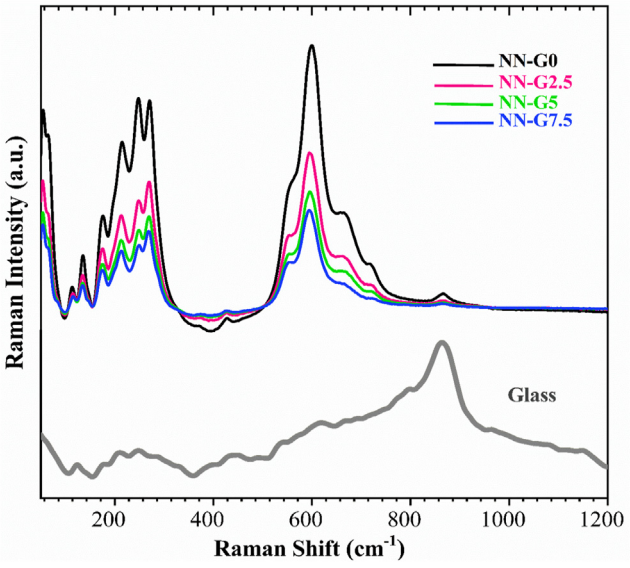

Figure 2. Raman spectra of the NNP glass, the ceramic NN and the composites (100-x)NN-xNNP.

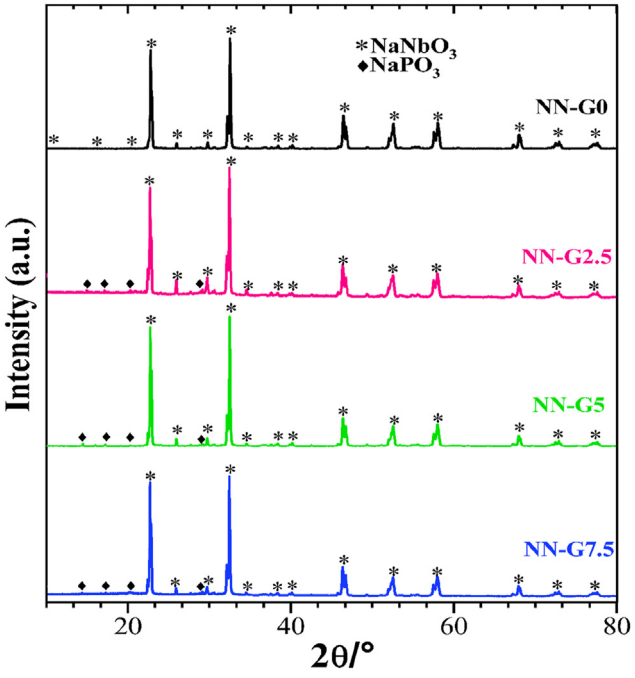

Figure 3. XRD patterns of the (100-x)NN-xNNP composites.

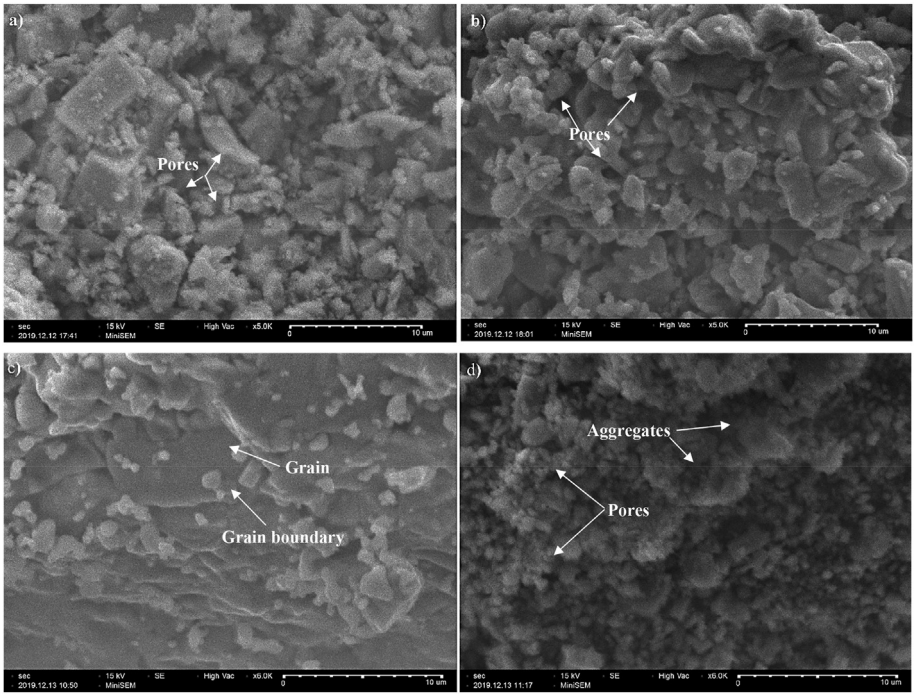

Figure 4. SEM micrographs of the polished surface of the composites (100-x) NN-xNNP; (a) NN- G0, (b) NN-G2.5, (c) NN- G5 and (d) NN- G7.5.

as shown in Figure 4 (b) leads to a reduction of the space between the grains and consequently to a partial decrease of the pores. The vitreous phase is generally located at the NN ceramic grain boundaries [8]. A similar glass effect is reported in the literature by the addition of a silicate glass to $BaTiO_3$ ceramic [19]. The NN-G5 composite has a uniform and denser microstructure as shown in Figure 4 (c) which can be explained by the homogeneity and the almost complete disappearance of the pores. The formation of this kind of microstructure could be due to the low melting temperature of the glass NNP which leads to the densification of the composite by the liquid phase sintering process [20]. Supplementary addition of glass up to 7.5 wt % as seen in Figure 4 (d) shows a decrease in density and the appearance of cracks and voids. This result is in agreement with the reported literature data on the sintering lithium niobate ceramics with glass additions [21]. From the obtained results, it can be concluded that incorporating 5 wt% of NNP glass has a dual effect on the NN ceramics microstructure. On the one hand, the grain size of the NN phase is considerably reduced; on the other hand, the pore size has decreased. This would have a positive impact on NN-Gx composites' dielectric properties.

Summarizing, the average grain size of the composites decreases with increasing NNP glass content (Figure 5) and then increases on a further increase of the glass content, specifically, for the highest NNP glass content (NN-G7.5). Two interesting results stand out from the study of the evolution of the GSD (Figure 5); at first, the NN-G0 and NN-G2.5 composites have a multimodal distribution of particle size, where bigger particle the particles are enclosed by small ones, such as; at second, if the NNP glass content rises, the GSD shifts toward a unimodal distribution. As a result, it is reasonable to conclude that adding glass to the device results in a more uniform particle distribution with much small particle size.

3.5. Dielectric properties

The dielectric properties, ε_r and tan δ, as a function of frequency from 100Hz to 1 MHz at room temperature of the NN-Gx composites sintered at 900 °C are represented in Figure 6(a-b). Many polarization mechanisms can occur in dielectrics such as electronic, ionic, dipole orientation, migration, and space charge. The polarization of the orientation and the polarization of a migration/space charge are frequency-dependent; and generally diminish at higher frequencies. It is well known that the orientation polarization depends on temperature and decreases owing to thermal agitation. The migration polarization is also temperature-dependent but increases with increasing temperature. Generally, in a dielectric, the permittivity is due to the rotation of ions around their negative sites and to short-range dipole transport. From the analysis of Figure 6 (a-b), it can be seen that the dielectric parameters increase rapidly with the decreasing frequency while they reach small independent frequency values at higher frequencies. The low-frequency region is linked to many factors that can influence the dielectric properties such as defects, fluctuation in composition, migration of charge carriers, space charge, and sample-electrode polarizations [22]. The accumulation of charge carriers in the composite-electrode interface does not allow the further transfer of charge carriers through the NN-Gx composites. In the high-frequency region, the effect of the periodic reversal electric field

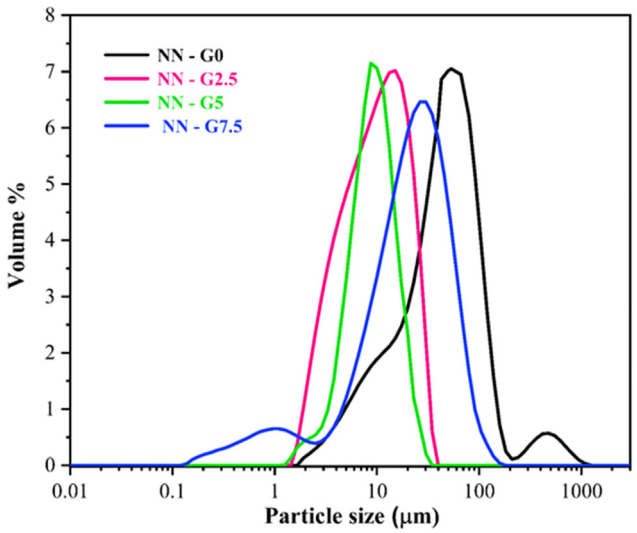

Figure 5. Particle size distributions of the composites (100-x) NN-xNNP.

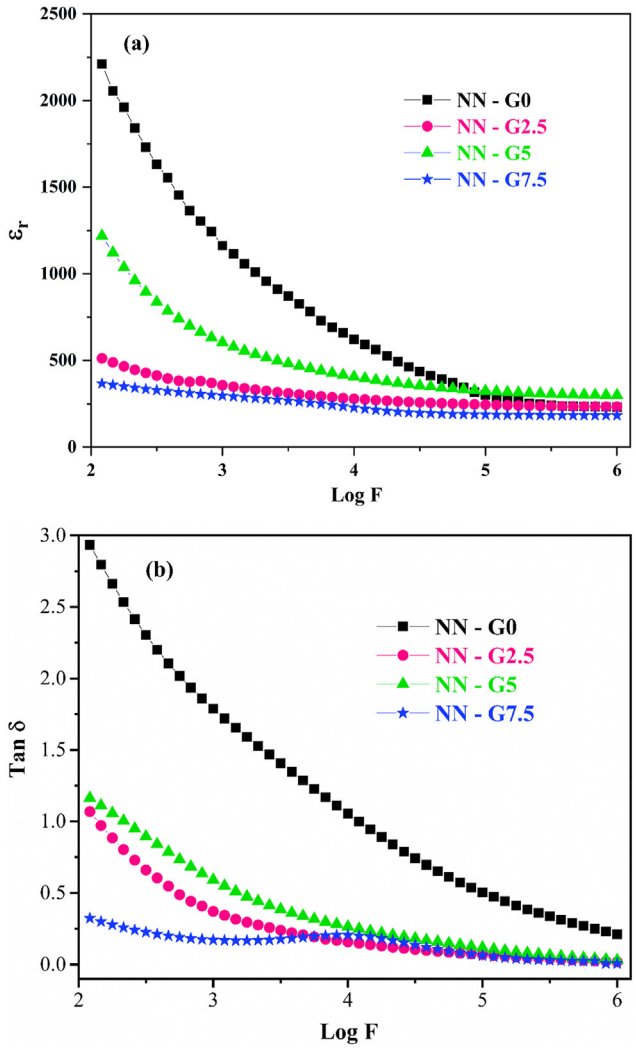

Figure 6. Frequency dependence of (a) the permittivity (εr) and (b) the dielectric loss (Tanδ) at RT of the composites (100-x)NN-xNNP.

occurs and provokes the decrease of the polarization issued from the space charge accumulation and causes a drop in the dielectric parameters. The dielectric constant of the pure ceramic NN is nearly 230.4 with losses up to 0.21 at 1MHz. Unfortunately, it is worth noticing that even this permittivity value is high, the pure ceramic NN had a low breakdown strength because of the existence of defects as pores and grain boundaries [2]. The addition of glass NNP had a significant role in improving the dielectric properties of NN-Gx composites at high frequencies. For example, the addition of 2.5 wt % and 5 wt % of NNP glass leads to an observable increase in the permittivity up to 406 and a decrease in losses down to 0.01. But the extra addition of glass 7.5 wt % negatively influenced the permittivity. The composite dielectric properties are related to their composition. The greater dielectric results are observed for NN-G5 composite. It had a good permittivity constant with low dielectric losses. This is because NN-G5 composite was distinguished by a dense microstructure because of the decrease in pores as shown in Figure 4. The diminishing dielectric constant for NN-G7.5 composite can be explained by the existence of the glassy phase excess and the formation of the secondary non-dielectric phase ($NaPO_3$) as illustrated in Figure 3.

The Figure 7 (a-b) demonstrate the relative permittivity (dielectric constant) and the dielectric loss of (100-x)NN-xNNP (x = 0, 2.5, 5, 7.5 mol %) composites as a function of temperature from 30 to 300 °C at 1 MHz. From these figures, it can be clearly seen that the variation of the dielectric constant of each sample is nearly independent of temperature up to 150 °C and then increase steeply until 300 °C. At a fixed temperature, the permittivity of the materials increases by up to 5 wt % addition of glass and then decreases with an addition of 7.5 wt %. The highest dielectric constant value is observed for the NN-G5 composite; it reaches 406.44 at RT with a dielectric loss of less than 0.01. From these results, it can be deduced that the incorporation of 5 wt % of the glass enhances the dielectric properties of the composites by minimizing the grain boundary leakage current, locking the conduction channels, and clamping the NN particles as shown in Figure 4. The decrease of the dielectric properties for a content glass up to 7.5% is due to its porous microstructure. The electrical parameters ε_r and tan δ at 1 MHz of the NN-Gx composites are presented in Table 1.

3.6. Energy storage performance

In general, for dielectric materials, the energy storage properties are described by three parameters calculated using the Eqs. (2), (3), and (4) [23]:

$$W_{rec} = \int_{Pr}^{Pmax} EdP \qquad (2)$$

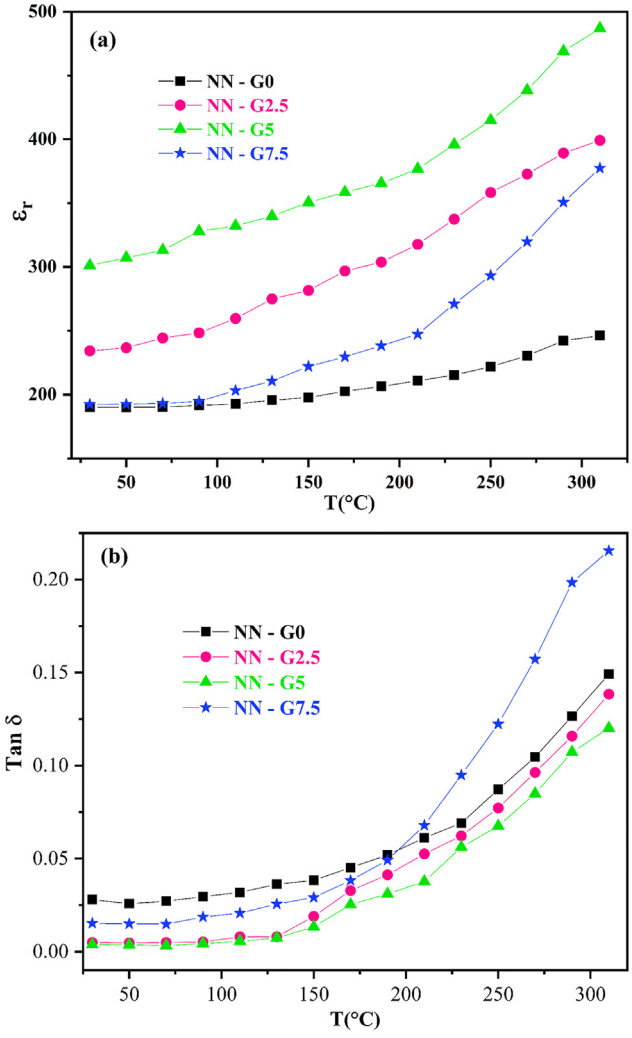

Figure 7. Temperature dependence of (a) the permittivity (εr) and (b) the dielectric loss (Tanδ) at 1MHz of the composites (100-x)NN-xNNP.

Table 1. The values of the dielectric parameters (ε_r) and (Tanδ) for the composite at different temperatures at 1 MHz.

sample	T (°C)	ε_r	Tan δ
NN-G0	30	230.49	0.14
	300	246.19	0.21
NN-G2.5	30	233.68	0.01
	300	399.27	0.13
NN-G5.0	30	406.44	0.01
	300	487.00	0.12
NN-G7.5	30	183.47	0.01
	300	377.48	0.21

$$W_{loss} = \int_0^{Pmax} EdP - Wrec \tag{3}$$

$$\eta = \frac{W_{rec}}{W_{rec} + W_{loss}} \times 100 \tag{4}$$

Where E, Pmax, Pr stands for the electric field, maximum polarization, and remnant polarization, respectively. W_{rec} is the energy density that can be recovered, it equal to the integral area between the polarization axis and the discharge curve in the P–E hysteresis loop. W_{loss} is the energy loss density which is the area of the P–E. The parameter η is the energy efficiency is defined as the ratio of the energy density released to the energy density stored, see Figure 8 (a). The calculated parameters of the P-E loops composites, W_{rec}, W_{loss}, and η, are summarized in Table 2.

Unfortunately, since the amplitude of the voltage in this system is small, the highest electric field that can be applied to the materials is 40 kV cm-1 at room temperature. This means that the composites' estimated energy density is significantly smaller than their actual density. The energy storage density is also underestimated since the hysteresis loop is tested at the high frequency of 5 kHz, which partially excludes the Maxwell Wagner-Sillars polarization measured at low frequencies. Many high-frequency applications, especially in electronics, benefit from the energy measured in these experimental conditions.

The P–E hysteresis loops of the composites (100-x)NN-xNNP are plotted in Figure 8 (a), Because of the limitation of the measuring device voltage amplitude, the composites hysteresis loops exhibit a lossy behavior due to the leakage current occurring in the samples. The source of this leakage current is due to defects that caused a hopping phenomenon [24]. From Figure 8 (a), it can be clearly seen that the pure NN displays a large remnant polarization of 0.03 μC/cm^2 and a Pmax of 1.31 μC/cm^2. Depending on the glass content added to the composite, the values of these two parameters differ as well as the shape of the loops P-E. From Figure 8 (a), it can be observed that with increasing NNP glass content to 5 wt %, the loops of the composite NN-G2.5 and NN-G5 become much slimmer than that of pure NN. By increasing the glass content up to 7.5 wt % the loop of NN-G7.5 composite becomes larger again.

The composition dependencies of the energy density (W_{rec}) and the energy loss (W_{loss}) of the composites are plotted in Figure 8 (b). It is seen that with increasing glass content up to 5 mol%, the W_{rec} increase while the W_{loss} decrease. The NN-G5 composite exhibits the higher recoverable energy density (W_{rec}) value of 68.4 mJ/cm^3 and the lower energy loss (W_{loss}) value of 12.2 mJ/cm^3 which yields an energy efficiency (η) value

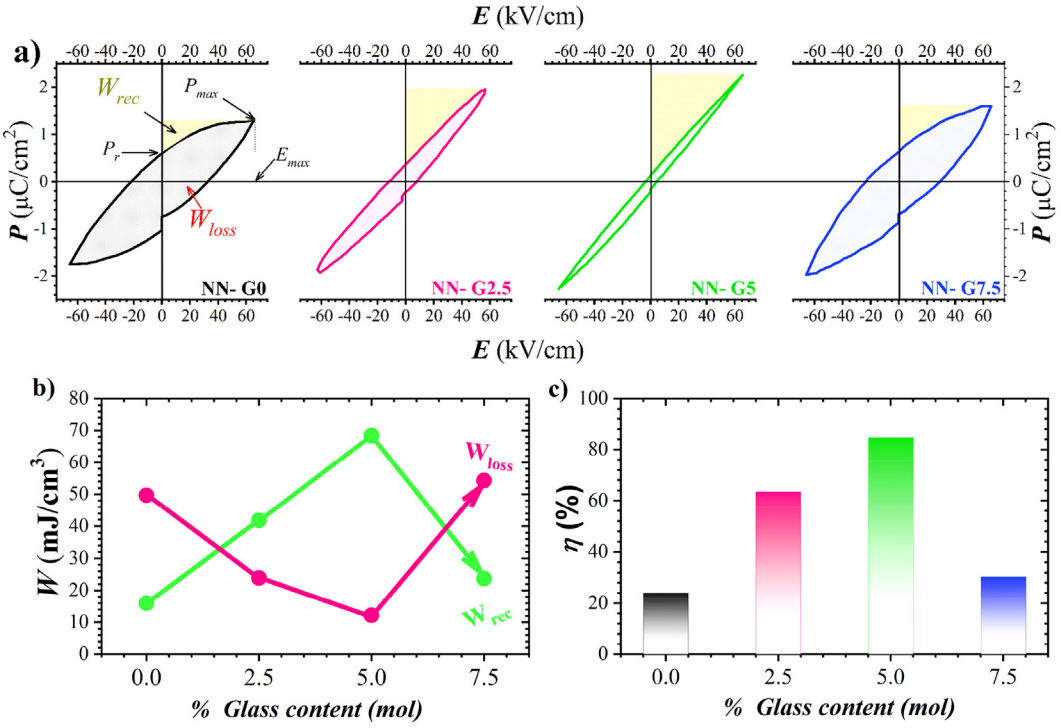

Figure 8. Energy storage performance of the (100-x) NN-x NNP composites: (a). P–E hysteresis loops of the composites as a function of the glass content at the electric field of 40 kV/cm, (b). The W_{rec} and W_{loss} evolution as a function of the incorporate glass content in the ceramic NN, (c). Energy efficiency (η) of the (100-x) NN-xNNP composites.

Table 2. Polarization and energy storage parameters of the composites at an electric field of 40 kV/cm.

Sample	P_r (μC/cm^2)	P_{max} (μC/cm^2)	W_{rec} (mJ/cm^3)	W_{loss} (mJ/cm^3)	η(%)
NN-G0	0.03	1.31	16.0	49.7	24.0
NN-G2.5	0.04	1.94	41.8	23.9	63.5
NN-G5.0	0.01	2.25	68.4	12.2	84.8
NN-G7.5	0.06	1.60	23.7	54.3	30.3

as high as ~ 84.8% at room temperature as shown in Figure 8 (c). With the further addition of NNP up to 7.5 mol% (NN-7.5), one can note that the recoverable energy density, energy loss, and the energy efficiency of the composite NN.7.5 decrease to 23.7 mJ/cm^3, 54.3 mJ/cm^3, and 30.3% respectively but still higher than the pure ceramic NN.

The addition of the NNP glass to NN ceramic can affect the energy storage performance for the (100-x)NN-xNNP composites. The enhancement of the NN-G2.5 and NN-G5 composites' energy density is explainable by considering the microstructure and SEM image (Figure 4), which indicated a reduction in grain size and a decrease in the amount of pores. This leads to a reduction in the trapping of free charge through the grain boundary and the pore that controls ferroelectric polarization. Furthermore, as the glass's content is increased, the polarization hysteresis loop is affected, lowering the value of the remnant and saturation polarization at the same time, resulting in a decrease in the energy storage density. Moreover, the addition of more glass can also damage the core-shell structure during the sintering process resulting in grain growth and secondary phase formation. For that, it is necessary to control the glass content added to a pure ceramic by controlling the composition in order to enhanced the composites energy storage performance.

4. Conclusion

The Na_2O–Nb_2O_5–P_2O_5 glass was added to the pure $NaNbO_3$ (NN) ceramic, it has positively affected the fritting temperature, microstructure, dielectric, and energy storage features of the NN ceramic. The obtained results revealed that the control of the ceramic microstructure is regulated by the amount of the introduced NNP glass. Specifically, it is found that the NN-G5 composite exhibited a high increase in permittivity and low dielectric losses, less than 0.01, and also a high improvement of the recoverable energy density reached 68.4 mJ/cm^3 with an efficiency energy of 84.8%. This behavior is due to the diminution of the porosity and defects existing in the NN ceramic as well as the reduction of the grain size which caused a synergistic effect with the NNP glass network to improve the dielectric properties of the composites. Regarding the actual results, one can conclude that the phosphate NNP glass is suitable to perform NN-based glass-ceramics which exhibits enhanced energy storage performance. The optimum content of the NNP glass in the composites was found 5%. Therefore, it can be concluded that NN-G5 glass-ceramic composite is an attractive dielectric candidate for energy storage capacitor ceramics.

Declarations

Author contribution statement

S. Benyounoussy: Conceived and designed the experiments; Performed the experiments; Analyzed and interpreted the data; Wrote the paper.

L. Bih: Conceived and designed the experiments; Contributed reagents, materials, analysis tools or data; Wrote the paper.

F.Muñoz: Contributed reagents, materials, analysis tools, or data; Wrote the paper.

F.Rubio-Marcos: Analyzed and interpreted the data; Wrote the paper.

A. EL Bouari: Conceived and designed the experiments; Contributed reagents, materials, analysis tools or data; Wrote the paper.

Funding statement

This work was supported by CNRST, Morocco, and OCP Foundation, Morocco in the framework of the Apphos project (Mat-Bih-01/2017. F. M). Dr Rubio-Marcos was supported by the AEI, Spain (Spanish Government) Projects (MAT2017-87035-C2-1-P and MAT2017-86450-C4-1-R), the "Ramon y Cajal" contract (RyC-2015-18626), which is co-financed by the European Social Fund, European Union and a 2018 Leonardo Grant for Researchers and Cultural Creators, BBVA Foundation, Spain.

Data availability statement

Data included in article/supplementary material/referenced in article.

Declaration of interests statement

The authors declare no conflict of interest.

Additional information

No additional information is available for this paper.

References

[1] Z. Yao, Z. Song, H. Hao, Z. Yu, M. Cao, S. Zhang, M.T. Lanagan, H. Liu, Homogeneous/inhomogeneous-structured dielectrics and their energy-storage performances, Adv. Mater. 29 (2017) 1601727.

[2] L. Eric Cross, P N S, in: E.L. Colla (Ed.), *Ferroelectric Ceramics: Tutorial Reviews, Theory, Processing, and Applications* ed B Basel: Birkhäuser Basel, 1993, p. 381.

[3] M. Zhou, R. Liang, Z. Zhou, X. Dong, Ultrahigh energy storage properties with excellent stability in novel $NaNbO_3$-based lead-free ceramics with A-site vacancy: through Bi_2O_3 substitution strategy, J. Mater. Chem. 6 (2018) 17896–17904.

[4] J. Ye, G. Wang, M. Zhou, N. Liu, X. Chen, S. Li, F. Cao, X. Dong, Excellent comprehensive energy storage properties of novel lead-free $NaNbO_3$-based ceramics for dielectric capacitor applications, J. Mater. Chem. C 7 (2019) 5639–5645.

[5] M. Benlahrache, N. Benhamla, S. Achour, Dielectric properties of $BaTiO_3$–$NaNbO_3$ composites, J. Eur. Ceram. Soc. 24 (2004) 1493–1496.

[6] V. Deshpande, M. Jagdale, Effect of Li_2O-B_2O_3-SiO_2-Nb_2O_5 glass addition on dielectric and ferroelectric properties of Lithium Niobate ceramics, Ferroelectrics 510 (2017) 195–202.

[7] E. Haily, L. Bih, A. Lahmar, M. Elmarssi, B. Manoun, Effect of BaO–Bi_2O_3–P_2O_5 glass additive on structural, dielectric and energy storage properties of $BaTiO_3$ ceramics, Mater. Chem. Phys. 241 (2020) 122434.

[8] Q. Zhang, L. Wang, J. Luo, Q. Tang, J. Du, Improved energy storage density in barium strontium titanate by addition of BaO–SiO_2–B_2O_3 glass, J. Am. Ceram. Soc. 92 (2009) 1871–1873.

[9] T. Li, H. Segawa, N. Ohashi, Sintering behavior and dielectric properties of $BaTiO_3$ added with BaO-Bi_2O_3-B_2O_3 glass phase, Ceram. Int. 44 (2018) 13004–13010.

[10] A. Flambard, J.-J. Videau, L. Delevoye, T. Cardinal, C. Labrugère, C. Rivero, M. Couzi, L. Montagne, Structure and nonlinear optical properties of sodium–niobium phosphate glasses, J. Non-Cryst. Solids 354 (2008) 3540–3547.

[11] Y. Juang, S. Dai, Y. Wang, W.-Y. Chou, J. Hwang, M. Hu, W. Tse, Phase transition of $LixNa1- xNbO_3$ studied by Raman scattering method, Solid State Commun. 111 (1999) 723–728.

[12] H. Ge, Y. Hou, C. Xia, M. Zhu, H. Wang, H. Yan, Preparation and piezoelectricity of $NaNbO_3$ high-density ceramics by molten salt synthesis, J. Am. Ceram. Soc. 94 (2011) 4329–4334.

[13] Z. Shen, X. Wang, M. Kuok, S. Tang, Raman scattering investigations of the antiferroelectric–ferroelectric phase transition of $NaNbO_3$, J. Raman Spectrosc. 29 (1998) 379–384.

[14] R. Lima, P. Freire, J. Sasaki, A. Ayala, F. Melo, J. Mendes Filho, K. Serra, S. Lanfredi, M. Lente, J. Eiras, Temperature-dependent Raman scattering studies in $NaNbO_3$ ceramics, J. Raman Spectrosc. 33 (2002) 669–674.

[15] T. Wu, Y. Pu, T. Zong, P. Gao, Microstructures and dielectric properties of Ba0. 4Sr0. 6TiO3 ceramics with BaO–TiO_2–SiO_2 glass–ceramics addition, J. Alloys Compd. 584 (2014) 461–465.
[16] D.-M. Smilgies, Scherrer grain-size analysis adapted to grazing-incidence scattering with area detectors, J. Appl. Crystallogr. 42 (2009) 1030–1034.
[17] J. Koruza, B. Malič, O. Noshchenko, M. Kosec, Top-down processing of $NaNbO_3$ nanopowder, J. Nanomater. (2012).
[18] X. Li, Q. Li, L. Wang, The effects of $NaNbO_3$ particle size on the photocatalytic activity for 2-propanol photodegradation, Phys. Chem. Chem. Phys. J. 15 (2013) 14282–14289.
[19] H.-I. Hsiang, C.-S. Hsi, C.-C. Huang, S.-L. Fu, Sintering behavior and dielectric properties of $BaTiO_3$ ceramics with glass addition for internal capacitor of LTCC, J. Alloys Compd. 459 (2008) 307–310.
[20] P. Gao, H. Ji, Q. Jia, X. Li, Low-temperature sintering and dielectric properties of $Ba_{0.6}Sr_{0.4}TiO_3$–MgO composite ceramics with CaO–B_2O_3–SiO_2 glass addition, J. Alloys Compd. 527 (2012) 90–95.
[21] V. Deshpande, M. Jagdale, Synthesis and characterization of lithium niobate ceramics with glass additions, Eur. J. Glasses Sci. Technol. B Phys. Chem. Glasses 57 (2016) 133–138.
[22] P. Tripathi, P. Kumari, V. Mishra, R. Singh, S. Singh, D. Kumar, Effect of PbO–B_2O_3–BaO–SiO_2 glass additive on dielectric properties of $Ba_{0.5}Sr_{0.5}TiO_3$ ceramics for radio-frequency applications, J. Phys. Chem. Solid. 127 (2019) 60–67.
[23] Z.-M. Dang, J.-K. Yuan, S. Yao, R. Liao, Preparation and dielectric properties of core-shell structured Ag@ polydopamine/poly (vinylidene fluoride) composite, Adv. Mater. 25 (2013) 6334–6365.
[24] Jae-Hwan Park, Byung-Kook Kim, Jae-Gwan Park, In-Tae Kim, Hae-June Je, Yoonho Klm, Soon Ja Park, Dielectric hysteresis measurement in lossy ferroelectrics, Ferroelectrics 230 (1) (1999) 151–156.